Quantum coherence of muons in copper (II) acetate

S. Athira,[1,*] Benjamin M. Huddart,[2] Stephen J. Blundell,[2] Roshini Thomas,[1] James S. Lord,[3] D. T. Adroja,[3,4] and D. Jaiswal-Nagar[1,†]

[1] *School of Physics, IISER Thiruvananthapuram, Vithura, Thiruvananthapuram-695551, India*
[2] *Clarendon Laboratory, University of Oxford, Department of Physics, Oxford OX1 3PU, United Kingdom*
[3] *ISIS Facility, Rutherford Appleton Laboratory, Chilton, Didcot Oxon OX11 0QX, United Kingdom*
[4] *Highly Correlated Matter Research Group, Physics Department, University of Johannesburg, PO Box 524, Auckland Park 2006, South Africa*

(Dated: February 11, 2026)

We report on muon-spin relaxation (μ^+SR) measurements of copper acetate ($Cu(CH_3CO_2)_2{\cdot}H_2O$), a model spin-1/2 Heisenberg antiferromagnetic dimer chain with an alternation parameter $\alpha = 0.001$. Zero-field μ^+SR data collected from **2 to 200 K** revealed an oscillatory asymmetry that was analyzed using a model based on the muon-stopping site determined by DFT+μ calculations. Below 50 K, the fitted parameters capture spin dynamics characteristic of the singlet ground state, while at higher temperatures, an additional relaxation was observed due to the thermally populated triplet state, affecting the local magnetic field around the muon-stopping site. The temperature dependence of the fitting parameters was found to exhibit characteristics similar to those of a bipartite entanglement measure, "distance between the states", obtained from the magnetic susceptibility data. Longitudinal-field μ^+SR measurements reveal field-dependent relaxation at field values much lower than the field values required to close the spin singlet-triplet gap, emphasising the importance of quantum fluctuations in the spin dynamics of the dimerized copper acetate.

Research on quantum magnets has emerged as a forefront of many-body quantum phenomena in condensed matter physics [1, 2]. In particular, one-dimensional (1D) $S = 1/2$ quantum magnets stand out [3] since quantum fluctuations are intensified in these systems due to the low dimensionality and low spin value [4], and also by magnetic frustration, which is commonly found in various molecular magnets [5]. To observe these effects experimentally, materials are needed that closely resemble theoretical models of low-dimensional quantum magnets. Spin-1/2 ions, such as Cu(II), are therefore widely employed in investigating the quantum properties of low-dimensional molecular magnets.

Molecular magnets with Cu(II) as the magnetic centers, arranged into spin chains, are often modeled by the Heisenberg antiferromagnetic chain (HAfc), governed by the Hamiltonian $\mathcal{H} = -J\sum_i \vec{S}_i{\cdot}\vec{S}_{i+1}$ where J is the nearest neighbor exchange constant along the spin chain [6, 7]. In systems where nearest-neighbor spins are coupled by alternating exchange constants, J_1 and J_2 ($J_2 \ll J_1$), the spin chain forms alternating strong and weak bonds, resulting in a spin-dimer HAfc [8–10]. The ratio $\alpha = J_2/J_1$ characterizes the strength of the magnetic interaction between the dimerized spins. The ground state of a dimerized HAfc system is a non-magnetic spin singlet, separated from a triplet excited state by a finite spin gap Δ [11]. Among the reported dimer materials [12–15], copper acetate offers the best experimental realisation of a dimerized HAfc, characterized by an exceptionally small α value of 0.001 [16]. This makes copper acetate an ideal model for testing theoretical predictions about quantum fluctuations in a dimerized HAfc using various experimental methods. Recent experimental studies have quantified the entanglement content of copper acetate using bipartite entanglement measures such as the distance between states, concurrence, and quantum discord [16, 17]. Since muon spin relaxation measurements can effectively pick-up low energy spin fluctuations and serve as a powerful probe for gaining deeper insights into microscopic spin dynamics, it is interesting to explore whether such bipartite entanglement signatures can be detected via muon spin relaxation (μ^+SR) measurements.

μ^+SR experiments [18] offer a microscopic view of magnetic ordering and spin dynamics in molecular magnetic systems and serve as an important technique for measuring local magnetism as well as fluctuations arising in the magnetic order [19–25]. As a classic example of a dimerized HAfc compound, copper acetate serves as an ideal model for studying spin dynamics in dimer systems using μ^+SR measurements. In this letter, we present the results of temperature-dependent μ^+SR measurements on copper acetate in both zero-field (ZF) and longitudinal-field (LF) configurations, where the observed relaxation function reveals temperature and field-dependent spin fluctuations. Furthermore, DFT+μ [26] calculations were utilized to identify muon-stopping sites, enabling the development of a theoretical model that was found to fit the ZF μ^+SR data very well. Additionally, magnetic susceptibility measurements were conducted on copper acetate crystals to compare μ^+SR results with a bipartite quantum entanglement measure, specifically the "distance between the states", $\mathcal{E}(\chi)$, demonstrating that quantum fluctuations linked to bipartite entanglement can be effectively detected via muon spectroscopy.

* athirasuresh20@iisertvm.ac.in
† deepshikha@iisertvm.ac.in

Single crystals of copper acetate ($Cu(CH_3CO_2)_2{\cdot}H_2O$) were synthesized via a slow evaporation method, where crystals gradually formed as the solvent evaporated from a supersaturated solution [16]. The prepared sample was then mounted onto a silver holder with vacuum grease and wrapped in silver foil. μ^+SR measurements were then conducted on this sample with the HiFi spectrometer at the Rutherford Appleton Laboratory, ISIS Facility in the UK. The sample was placed on the sample stick of a ^{4}He cryostat in the HiFi instrument, and data were collected across a temperature range from 2 to 200 K for zero-field (ZF) measurements. Spin-polarized positive muon pulses are produced every 20 ms at the ISIS facility, with a full width at half maximum (FWHM) of 70 ns. These muons are implanted into the sample, where they decay into positrons with a half-life of 2.2 μs. The experimentally measured quantity is the forward-backward asymmetry, $A(t)$, that represents the difference in positron count rates between the forward and backward directions relative to the initial muon spin polarization. It is directly proportional to the instantaneous spin polarization of the muon ensemble projected along the initial muon beam direction, $A(t) = A_0 P_z(t)$ with A_0 being the instrumental asymmetry [27]. Measurements were also performed in an applied longitudinal field (LF), with the magnetic field aligned parallel to the initial muon spin direction. LF measurements were taken at fixed temperatures below 200 K, with magnetic fields ranging up to 4 T. Furthermore, magnetization measurements were done on a 10 mg crystal on Quantum Design's superconducting quantum interface device (SQUID) magnetometer (Model MPMS3) in the temperature range of 2 K to 300 K.

We have carried out DFT+μ calculations using the plane-wave basis-set electronic structure code CASTEP [28] in order to determine the muon-stopping sites. Calculations were carried out within the generalized-gradient approximation (GGA) using the PBE functional [29]. Copper (II) acetate crystallizes in the monoclinic $C2/c$ (No. 15) space group, with $a = 13.1585(8)$ Å, $b = 8.5575(5)$ Å, $c = 13.8517(9)$ Å, and $\beta = 117.035(2)°$. Due to the relatively large size of the unit cell, structural relaxations with the muon were carried out on a single unit cell. Supercells are often used in these calculations to suppress the unphysical interaction of the muon with its periodic images in plane-wave DFT; the large unit cell size for this system means that this is unlikely to be necessary here. We used a plane-wave cutoff energy of 900 eV and $2\times1\times2$ Monkhorst-Pack grid [30] for Brillouin zone sampling, resulting in total energies that converge to within 1 meV per atom. The system was treated as non-spin-polarized in these calculations.

Figs. 1(a) and (b) show the time evolution of positron decay asymmetry $A(t)$ obtained from ZF μ^+SR measurements on the copper (II) acetate sample, between the temperature range of 2 and 200 K. A clear oscillatory behavior is apparent in the 2 K data which persists, albeit with more damping, up to higher temperatures. While such spontaneous oscillations of muon polarisation in magnetic materials are indicative of the magnetic field resulting from a magnetic order [31], this is clearly not the case for copper acetate, as it shows no evidence of magnetic order down to 2 K. Previous thermodynamic measurements have demonstrated that at low temperatures, the sample exhibits no magnetic ordering, but all Cu^{2+} dimers are in singlet states, thereby, producing zero net magnetic field at the muon site [16], precluding a precession signal. However, oscillatory signals have also been observed in alkali metal fluorides, where they occur in the absence of magnetic ordering [32, 33]. In this case, the oscillations arise from the formation of a local atomic cluster consisting of the muon and a small group of neighboring atoms with nuclear magnetic moments. These nuclear moments cause the muon spin to undergo precession. It is, therefore, highly likely that the observed oscillations in copper acetate result from entanglement between the muon spin and nearby nuclei, most likely protons, as commonly seen in nonmagnetic or paramagnetic materials [34, 35]. Therefore, in order to understand the observed μ^+SR data better, we carried out DFT + μ calculations (described above) to find the lowest energy muon site. From the calculations, the muon stopping sites were found to belong to five distinct classes based on the local environment of the muon. The details of these sites, along with the corresponding energies, are tabulated in Table I of Appendix A.

As shown in Table I, it was found that at the lowest energy muon site A, the muon sits between two O atoms with unequal μ–O bond lengths of 1.07 Å and 1.45 Å. One of these O atoms belongs to a water molecule that is bonded to Cu, and the muon is therefore also quite close to two hydrogen atoms, with μ–H distances of 1.86 Å and 2.01 Å and a H–μ–H bond angle of 49°. The second oxygen atom at the muon site is contributed by the acetate group in the adjacent dimer unit. Consequently, the formation of the O–μ–O state results in the lengthening of the Cu–O bond to the water group, from 2.15 Å to 2.63 Å. The muon-site A is shown in Fig. 1 (c) with the bend H–μ–H "bonds". The dotted lines in the inset of Fig. 1 (c) shows the weak hydrogen "bonds" between two spin dimers as well as μ-H.

Due to the positive charge of the muon, it is expected to preferentially localize near negatively charged atoms [31] (oxygen in this case), which is confirmed from the lowest energy site A obtained from the DFT+μ calculations. However, the ^{16}O has zero nuclear spin, so the nuclei that are most likely to interact with the muon are the nearest spin-$\frac{1}{2}$ protons (^{1}H) from the water molecules in copper acetate. Therefore, the small oscillation observed in ZF measurements on copper acetate can be attributed to dipole-dipole interactions between the magnetic moments of the muon ($S = 1/2$) and the ^{1}H nuclei ($I = 1/2$). In this case, the oscillations might be expected to be similar to the well-known F–μ–F oscillations that are observed in fluorides [32], but with coupling to protons instead of fluorine in a non-collinear arrangement (bent

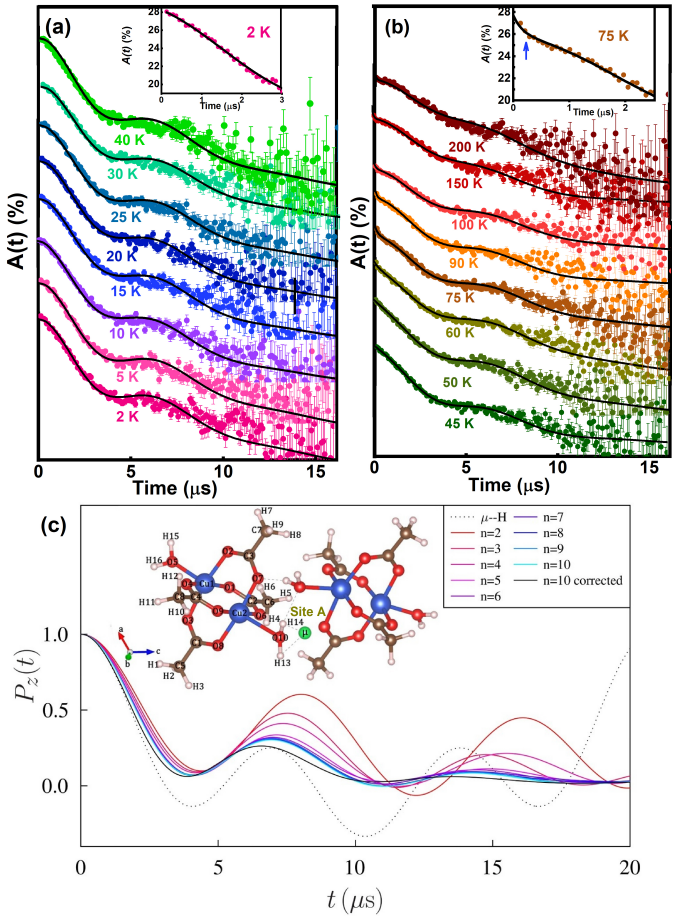

FIG. 1. Coloured circles represent the experimental muon decay asymmetry $A(t)$ (with arbitrary offset) in ZF measurement for temperatures (a) below T = 45 K and (b) above 45 K. ZF data is displayed on an expanded scale to compare the initial relaxation with the higher temperature data at 2 K and 75 K in the insets of (a) and (b) respectively. Arrow indicated the initial fast decay in (b). Black curves in (a) - (b) represent fits to the equation 3. (c) Polarization function, $P_z(t)$ given by equation 2 (see text for details) calculated for n neighbouring protons around the muon site. Inset shows the lowest energy muon site A in copper acetate obtained from DFT + μ calculations and shown inside the copper acetate unit cell with the two μ–H "bonds".

H–μ–H configuration) [33].

Under the assumption that the muon is most strongly coupled to two nearby protons, we can describe the resulting H–μ–H state by the Hamiltonian $\mathcal{H}$ which is written as

$$\mathcal{H} = \mathcal{H}_{\mu\mathrm{H}} + \mathcal{H}_{\mathrm{HH}}. \tag{1}$$

This is the sum of two terms containing: (1) $\mathcal{H}_{\mu\mathrm{H}}$ – dipolar interaction between the muon (spin $\boldsymbol{S}_\mu$) and the protons (spins $\boldsymbol{S}_{\mathrm{H1}}$ and $\boldsymbol{S}_{\mathrm{H2}}$) and (2) $\mathcal{H}_{\mathrm{HH}}$ – dipolar interaction between the two protons. Details of $\mathcal{H}_{\mu\mathrm{H}}$ and $\mathcal{H}_{\mathrm{HH}}$ can be found in Appendix B.

The polycrystalline average polarization calculated from the Hamiltonian is given by

$$P_z(t) = c_0 + \sum_{i=1}^{N} c_i \cos(\alpha_i t), \tag{2}$$

with the constants c_i and α_i determined by the geometry of the site. In the real crystal, there are, of course, many more distant nuclei that could be included in this model, so that the effect of other nuclei can add to an effective decohering background [36]. The effect of this is shown in Fig. 1(c), which plots the effect of including coupling to n additional neighboring protons, using the positions determined by the DFT+μ calculations. The $n = 2$ curve shows the dominant effect of the two protons in the H-μ-H cluster, which greatly improves on the $n = 1$ μ-H system (dotted line). Including additional protons increases the frequency and the damping, becoming closer to the 2 K data in Fig. 1(a), but still failing to match the observed behavior. The calculation of the $n = 10$ system is computationally intensive, requiring the diagonalising of 2048×2048 matrices, and including more remote nuclei (or indeed the $I = \frac{3}{2}$ Cu nuclei, which also have a quadrupolar interaction with the lattice) becomes unfeasible. Nevertheless, following the approach in [36], by enhancing the size of the nuclear moments on nuclei $3, 4, \ldots, 10$ by a factor 1.254, the truncated van Vleck sum (proportional to $\sum_i \mu_i^2 r_i^{-6}$) matches the sum obtained for the infinite crystal. This method quantifies the magnitude of the effect of the other moments and yields the black curve [labelled $n = 10$ corrected in Fig. 1(c), hereafter called $f(t)$], whose frequency matches the data very well, strongly supporting our interpretation. Although this accounts for much of the observed relaxation, the data shows slightly stronger relaxation, so that we fit our data using the function

$$G_z(t) = A_1 f(t) e^{-\lambda_1 t} + A_2 e^{-\sigma^2 t^2} + A_{\mathrm{bg}} + A_3 e^{-\lambda t} \tag{3}$$

where λ_1 is an additional exponential relaxation, the second (Gaussian) term models an additional slow relaxation, and we include a non-relaxing background A_{bg}. λ and A_3 indicate additional exponential relaxation that was found to arise at temperatures 50 K and above. Solid curves in Figs. 1 (a)-(b) represent the fits to the experimentally obtained ZF μ^+SR data using the asymmetry function, $G_z(t)$, obtained in equation 3 above. The constants c_i's and α_i's in equation 2 were fixed by incorporating the slightly different bond-lengths for the two μ–H "bonds" and a bond angle of 49° (very different from the 180° bond angle in a linear H–μ–H configuration) at the site A, leaving only the amplitudes A_i, width of the Gaussian σ, and the relaxation rate λ_1 as fitting parameters. The excellent agreement between the theoretical model and the experimental data confirms that the calculated muon site is highly plausible and consistent with the data. With these parameters, it was found that the ZF μ^+SR could be fitted for the temperature range 2 to 45 K using only the first three terms of equation 3 ($A_3 = \lambda = 0$) which were fixed to their following average values: $A_2 = 10\%$, $A_{\mathrm{bg}} = 8\%$, λ_1

$= 0.018\ \mu s^{-1}$ and $\sigma = 0.108\ \mu s^{-1}$. The fits suggest that below 40 K, the temperature is insufficient to produce triplet excitations of the copper dimers and so there is essentially no electronic magnetism. A significant fraction of the muons are in site A and couple to the nuclear moments, resulting in the oscillatory signal that matches the theoretical calculation very closely. Increasing temperature in this regime, from 2 K to 40 K, has very little effect. There is also a fraction of muons at some other site, which we are modelling by a Gaussian function, although we cannot rule out the possibility that this component is an artefact of some additional relaxation at the original site, which comes about from the effect of the (more distant) Cu nuclear moments.

Temperature variation of the fitting parameters A_1 and λ obtained by fitting the equation 3 is shown in Fig. 2 (a). From the figure, it can be seen that the amplitude A_1 of $f(t)$ (green open triangles) shows a very weak temperature dependence till 50 K above which it falls appreciably. Since the parameter A_1 measures the fraction of muons in the diamagnetic state, a fall in A_1 with increasing temperature above T^* indicates a loss in this fraction due to fluctuations out of the ground state from nearby copper dimers. Very interestingly, the parameter associated with an additional exponential decay of the asymmetry data, λ, starts to become finite at 50 K and above (open blue circles in Fig. 2) where $A_3 = 2.1\%$. From the ZF μ^+SR data of Fig. 1, it can be found that at temperatures 50 K and above, the asymmetry data have an additional initial fast decay. A representative expanded plot of the asymmetry data showing the fast initial decay is shown in the inset of Fig. 1 (b) measured at 75 K. Such an additional decay in the asymmetry was found to be absent for temperatures below 50 K (see the inset of Fig. 1 (a)). These observations are consistent with the onset of an additional source of relaxation at higher temperatures, most likely due to fluctuating electronic moments resulting from triplet excitations of the Cu dimers. Remarkably, the delicate quantum coherence that results from the muon coupling with nearby nuclear moments is preserved, which sets stringent limits on the static and fluctuating magnetic field at the muon site resulting from the triplet excitations arising from the Cu-Cu dimerized ground state.

In order to relate this observed behavior to the entanglement in the dimers, we measured *dc* magnetic susceptibility in copper acetate as shown by the filled red circles in Fig. 2 (b). From the figure, it can be seen that the magnetic susceptibility is zero till $\sim$ 50 K and starts to increase beyond that, consistent with previous reports [16, 37]. It is to be noted that this increase in magnetic susceptibility happens at the same temperature at which the exponential decay parameter of the asymmetry (A_3) data, λ, starts to rise. Since copper acetate offers an excellent system for studying bipartite entanglement [16], we calculated "distance between the state", $\mathcal{E}(\chi)$, given by $\mathcal{E}(\chi) = \max\left[0, 1 - 3\chi\frac{k_B T}{N_A(g\mu_B)^2}\right]$ [16, 38], a

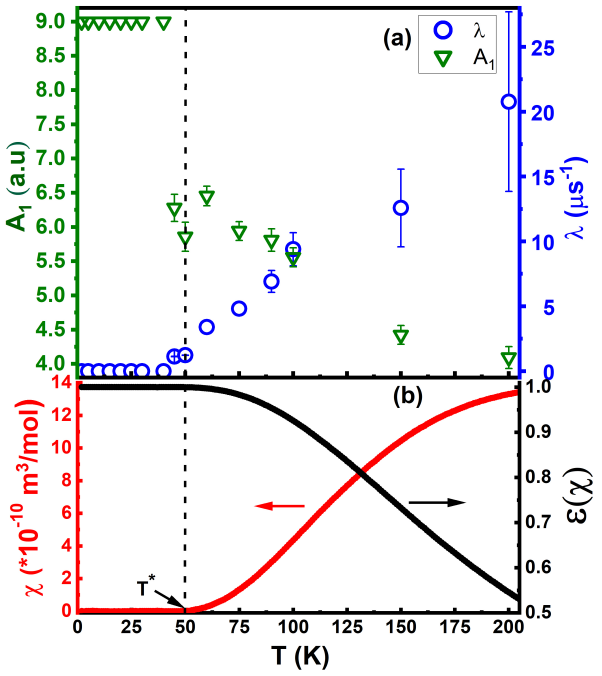

FIG. 2. (a) Green open triangles and blue open circles represent the temperature variation of fitted parameter A_1 and λ respectively (see text for details). (b) red filled circles denote the temperature variation of *dc* magnetic susceptibility, χ, measured on copper acetate at an applied magnetic field $\mu_0 H = 500$ mT. The rise of χ above the zero value is denoted by an arrow at a temperature T*. Black circles represent bipartite entanglement measure "distance between states", $\mathcal{E}(\chi)$.

good measure for bipartite entanglement. Black filled circles in Fig. 2(b) denote the temperature variation of, $\mathcal{E}(\chi)$, which starts from its maximum value 1 and starts to decrease at the same temperature where A_1 starts to decrease and λ starts to increase (see Fig. 2 (a)), pointing to the strong effect of entanglement present in this dimer system [16]. **In order to ensure that the loss in A_1 is not an artifact arising due to switching on an extra parameter A_3 in equation 3 and is correlated to the loss of the singlet state in the dimer, we calculated the temperature dependence of the singlet and triplet population and compared them with the temperature dependence of A_1 and the bipartite entanglement measure as shown in Fig. S1 of Supplemental Material (SM). From the figure, it can be seen that the reduction of A_1 occurs at precisely the temperature where the singlet population and $\mathcal{E}(\chi)$ begin to decrease.** Thus, the maximally entangled state exists till $\sim$ 50 K, beyond which population of the triplet state results in a decrease in entanglement and appearance of non-zero electronic spins in the electronic singlet background, generating dynamic local magnetic fields around the muon site and causing a faster relaxation, signifying a concomitant

increase in quantum fluctuations out of the singlet ground state.

Longitudinal field measurements were also performed (see SM Figs. S2 and S3) and show that the oscillatory component is quenched in rather small fields ($\sim$ 0.01 T) but that there are additional relaxation processes that persist even up to very high longitudinal fields (the highest measured was 4 T). The temperature and field variation of the fit parameters are described in SM Figs. S4 and S5. These results are consistent with our interpretation of the oscillatory component being nuclear in origin, but also demonstrate that there are additional relaxation processes which may be associated with quantum entanglement in this quasi-one dimensional spin 1/2 dimer system.

In conclusion, we conducted zero-field (ZF) and longitudinal-field (LF) μ^+SR measurements along with DFT+μ theoretical calculations to identify the muon-stopping site in copper acetate crystals. Our calculations revealed that the lowest-energy muon site corresponds to a non-linear H-μ-H configuration. Asymmetry function calculated from the theoretical model was found to fit the μ^+SR data very well below 50 K. Above 50 K, an additional initial relaxation in the ZF μ^+SR data indicated the presence of quantum fluctuations possibly arising due to the excitation of the triplet state. Comparison with a bipartite measure of quantum entanglement, namely, "distance between the states", $\mathcal{E}(\chi)$, revealed the loss of $\mathcal{E}(\chi)$ till those temperatures at which the parameters associated with ZF μ^+SR relaxation also decreased. Furthermore, LF μ^+SR measurements indicated the suppression of the relaxation due to nuclear contributions at an applied magnetic field of approximately 0.5 T. Similar to the ZF μ^+SR case, an extra relaxation was also obtained in the LF μ^+SR data above 50 K. Magnetic field variation of this relaxation parameter exhibited a finite value between 2-4 T, much lower than the spin excitation gap of copper acetate, indicating the possible effect of quantum entanglement in copper acetate.

Acknowledgments-D.J-N. acknowledges financial support from SERB, DST, Govt. of India (Grant No. CRG/2021/001262) and IGSTC Women Involvement in Science and Engineering Research (WISER) (Grant No. IGSTC/WISER 2024/DJN-2120/45/2024-25/89). Computing resources were provided by the STFC Scientific Computing Department's SCARF cluster. Work at Oxford was funded by UK Research and Innovation (UKRI) under the UK government's Horizon Europe funding guarantee [Grant No. EP/X025861/1]. We thank ISIS Facility for beam time on HiFi RB2310696, Ref. [https://doi.org/10.5286/ISIS.E.RB2310696].

Appendix A: Muon sites

Muon site calculations were carried out using the MuFinder program [39]. Initial structures comprising a muon (modelled as a proton) and the Cu (II) acetate unit cell were generated by requiring the muon to be at least 1.0 Å away from each of the initial muon positions in the previously generated structures (including their symmetry equivalent positions) and at least 1.0 Å away from any of the atoms in the cell. This resulted in 97 structures which were subsequently allowed to relax until the calculated forces on the atoms were all $< 5\times10^{-2}$ eV Å^{-1} and the total energy and atomic positions converged to within 2×10^{-5} eV per atom and 1×10^{-3} Å, respectively. Ignoring any sites with energies greater than 1 eV higher than the lowest energy site, we obtain 18 crystallographically distinct muon-stopping sites. Table I lists the possible muon sites from the calculations. The most probable site, labeled A, is described in the main text. Another site, denoted B, is only 0.4 meV higher in energy than the lowest energy site. This site is chemically equivalent to site A (and hence effectively identical in energy) but involves the muon taking the place of one of the hydrogen atoms in the water group, with the displaced hydrogen then forming an O–H–O state. These two sites will differ slightly in energy once the zero-point energy is taken into account, since a muon will have a larger zero point energy (ZPE) than a proton in the same environment as a result of its smaller mass. However, the change in ZPE upon swapping the positions of the muon and a proton is likely to be much smaller than the energy required to break an O-H bond in order to realize site B, and we therefore expect that site A is more likely to be realized in practice. Site C also involves substituting a hydrogen with the implanted muon, but this time the hydrogen belongs to a methyl group. Once again the displaced hydrogen forms an O–H–O state. In site D, the muon bonds to a single O atom with a μ–O bond distance of 1.0 Å. This significantly disrupts a Cu–O bond, with the Cu–O distance increasing from 1.95 Å to 3.10 Å. Site E involves the muon breaking the bond between oxygen and the methyl group and forming a CH_3-μ unit. However, this site is unlikely to form, given it is 0.643 eV higher in energy than the lowest energy site and requires

TABLE I. Muon stopping sites in copper (II) acetate obtained from DFT+μ using the structural relaxation method. Also shown are the energies of these sites, E, relative to the lowest energy site.

Site label	Fractional coordinates	E (eV)
A	(0.873 0.120 0.743)	0.0000
B	(0.950 0.279 0.708)	0.0004
C	(0.158 0.437 0.166)	0.1440
D	(0.146 0.907 0.997)	0.2350
E	(0.078 0.499 0.296)	0.6432

the breaking of bonds. Therefore, site A is expected to be the most likely realized in practice, as it has the lowest energy and does not require breaking any chemical bonds. Consequently, only this site was considered in our analysis.

Appendix B: Hamiltonian and Polarization function

The first term (1) in the Hamiltonian, given in equation 1, can be written as

$$\mathcal{H}_{\mu\mathrm{H}} = \frac{\mu_0}{4\pi}\sum_{i=1}^{2}\frac{\hbar^2\gamma_\mu\gamma_\mathrm{H}}{r_i^3}\left[\boldsymbol{S}_\mu\cdot\boldsymbol{S}_{\mathrm{H}i} - \frac{3(\boldsymbol{S}_\mu\cdot\boldsymbol{r}_i)(\boldsymbol{S}_{\mathrm{H}i}\cdot\boldsymbol{r}_i)}{r_i^2}\right] \tag{B1}$$

where $\boldsymbol{r}_i$ is the vector joining the muon and i^{th} proton and γ_μ and γ_H are the gyromagnetic ratios of the muon and proton, respectively; and (2) the dipolar interaction between the two protons

$$\mathcal{H}_{\mathrm{HH}} = \frac{\mu_0}{4\pi}\frac{\hbar^2\gamma_\mathrm{H}^2}{r_{\mathrm{HH}}^3}\left[\boldsymbol{S}_{\mathrm{H}1}\cdot\boldsymbol{S}_{\mathrm{H}2} - \frac{3(\boldsymbol{S}_{\mathrm{H}1}\cdot\boldsymbol{r}_{\mathrm{HH}})(\boldsymbol{S}_{\mathrm{H}2}\cdot\boldsymbol{r}_{\mathrm{HH}})}{r_{\mathrm{HH}}^2}\right] \tag{B2}$$

where $\boldsymbol{r}_{\mathrm{HH}}$ is the vector joining the two protons. The polycrystalline average polarization is then given by calculating the trace of the time-evolved density matrix multiplied by the appropriate spin operator [40] and the polycrystalline average of this gives an expression of the form

$$P_z(t) = c_0 + \sum_{i=1}^{N} c_i\cos(\alpha_i t), \tag{B3}$$

with the constants c_i and α_i determined by the geometry of the site. The $N \leq 8$ terms in the sum are due to the eight energy levels resulting from the coupling of the three spin-$\frac{1}{2}$ particles (N can be less than 8 if there are degenerate energy levels, which will occur for particular geometries of the H–μ–H system). This approach can be extended if further proton spins are included, though the Hamiltonian matrix becomes $2^{n+1}\times 2^{n+1}$ if n proton spins are included in addition to the muon spin.

[1] L. Amico, R. Fazio, A. Osterloh, and V. Vedral, Entanglement in many-body systems, Reviews of modern physics **80**, 517 (2008).

[2] G. Mathew, S. L. L. Silva, A. Jain, A. Mohan, D. T. Adroja, V. G. Sakai, C. V. Tomy, A. Banerjee, R. Goreti, A. V. N, *et al.*, Experimental realization of multipartite entanglement via quantum fisher information in a uniform antiferromagnetic quantum spin chain, Physical Review Research **2**, 043329 (2020).

[3] A. Pires and M. Gouvêa, Quantum fluctuations in low-dimensional easy-plane spin models, Eur. Phys. J. B **44**, 169–174 (2005).

[4] S. Sachdev, Quantum phase transitions, Physics world **12**, 33 (1999).

[5] F. L. Pratt, T. Lancaster, P. J. Baker, S. J. Blundell, W. Kaneko, M. Ohba, S. Kitagawa, S. Ohira-Kawamura, and S. Takagi, Muon spin relaxation studies of critical fluctuations and diffusive spin dynamics in molecular magnets, Physica B: Condensed Matter **404**, 585 (2009).

[6] M. Takahashi, *Thermodynamics of One-Dimensional Solvable Models* (Cambridge University Press, 1999).

[7] U. Schollwöck, J. Richter, D. J. J. Farnell, and R. F. Bishop, *Quantum magnetism*, Vol. 645 (Springer, 2008).

[8] B. Bleaney and K. D. Bowers, Anomalous paramagnetism of copper acetate, Proc. R. Soc. Lond. A **214**, 451 (1952).

[9] K. Ghoshray, B. Pahari, B. Bandyopadhyay, R. Sarkar, and A. Ghoshray, ^{51}V nmr study of the quasi-one-dimensional alternating chain compound $BaCu_2V_2O_8$, Phys. Rev. B **71**, 214401 (2005).

[10] D. Urushihara, S. Kawaguchi, K. Fukuda, and T. Asaka, Crystal structure and magnetism in the S= 1/2 spin dimer compound $NaCu_2VP_2O_{10}$, IUCrJ **7**, 656 (2020).

[11] C. P. Landee and M. M. Turnbull, Review: A gentle introduction to magnetism: units, fields, theory, and experiment, Journal of Coordination Chemistry **67**, 375 (2014).

[12] P. J. Baker, S. J. Blundell, F. L. Pratt, T. Lancaster, M. L. Brooks, W. Hayes, M. Isobe, Y. Ueda, M. Hoinkis, M. Sing, *et al.*, Muon-spin relaxation measurements on the dimerized spin- chains $NaTiSi_2O_6$ and $TiOCl$, Physical Review B—Condensed Matter and Materials Physics **75**, 094404 (2007).

[13] T. Lancaster, P. A. Goddard, S. J. Blundell, F. R. Foronda, S. Ghannadzadeh, J. S. Möller, P. J. Baker, F. L. Pratt, C. Baines, L. Huang, *et al.*, Controlling magnetic order and quantum disorder in molecule-based magnets, Physical Review Letters **112**, 207201 (2014).

[14] J. Xu, A. Assoud, N. Soheilnia, S. Derakhshan, H. L. Cuthbert, J. E. Greedan, M. H. Whangbo, and H. Kleinke, Synthesis, structure, and magnetic properties of the layered copper (ii) oxide $Na_2Cu_2TeO_6$, Inorganic chemistry **44**, 5042 (2005).

[15] Z. He, T. Kyômen, and M. Itoh, $BaCu_2V_2O_8$: Quasi-one-dimensional alternating chain compound with a large spin gap, Physical Review B **69**, 220407 (2004).

[16] S. Athira, S. L. L. Silva, P. Nag, S. Lakshmi, S. Kumar, D. P. Panda, S. Das, S. Rajput, A. P. Alex, A. Sundaresan, *et al.*, Bipartite entanglement via distance between the states in a one dimensional spin 1/2 dimer copper acetate monohydrate, New Journal of Physics **25**, 103002 (2023).

[17] M. A. Yurishchev, Quantum discord in spin-cluster materials, Phys. Rev. B **84**, 024418 (2011).

[18] S. Blundell, R. De Renzi, T. Lancaster, and F. L. Pratt, *Muon spectroscopy: an introduction* (Oxford University Press, 2022).

[19] J. M. Wilkinson, S. J. Blundell, S. Biesenkamp, M. Braden, T. C. Hansen, K. Koteras, W. Grochala, P. Barone, J. Lorenzana, Z. Mazej, *et al.*, Low-temperature magnetism of $KAgF_3$, Physical Review B **107**, 144422 (2023).

[20] F. L. Pratt, S. J. Blundell, T. Lancaster, C. Baines, and S. Takagi, Low-temperature spin diffusion in a highly ideal S= 1/2 heisenberg antiferromagnetic chain studied by muon spin relaxation, Physical Review Letters **96**, 247203 (2006).

[21] S. F. J. Cox, Implanted muon studies in condensed matter science, Journal of Physics C: Solid State Physics **20**, 3187 (1987).

[22] P. D. De Réotier and A. Yaouanc, Muon spin rotation and relaxation in magnetic materials, Journal of Physics: Condensed Matter **9**, 9113 (1997).

[23] F. Pratt, F. Lang, W. Steinhardt, S. Haravifard, and S. Blundell, Spin dynamics, entanglement, and the nature of the spin liquid state in $YbZnGaO_4$, Physical Review B **106**, L060401 (2022).

[24] H. C. Wu, F. L. Pratt, B. M. Huddart, D. Chatterjee, P. A. Goddard, J. Singleton, D. Prabhakaran, and S. J. Blundell, Spin dynamics in the dirac $u(1)$ spin liquid $YbZn_2GaO_5$, arXiv preprint arXiv:2502.00130 (2025).

[25] T. Lancaster, S. J. Blundell, M. L. Brooks, P. J. Baker, F. L. Pratt, J. L. Manson, and C. Baines, Muon-spin relaxation study of the spin-1 2 molecular chain compound $Cu(HCO_2)_2(C_4H_4N_2)$, Physical Review B—Condensed Matter and Materials Physics **73**, 172403 (2006).

[26] S. J. Blundell and T. Lancaster, Dft+ μ: density functional theory for muon site determination, Applied Physics Reviews **10** (2023).

[27] S. J. Blundell, Spin-polarized muons in condensed matter physics, Contemporary Physics **40**, 175 (1999).

[28] S. J. Clark, M. D. Segall, C. J. Pickard, P. J. Hasnip, M. I. J. Probert, K. Refson, and M. C. Payne, First principles methods using CASTEP, Z. Kristallogr. Cryst. Mater **220**, 567 (2005).

[29] J. P. Perdew, K. Burke, and M. Ernzerhof, Generalized gradient approximation made simple, Phys. Rev. Lett. **77**, 3865 (1996).

[30] H. J. Monkhorst and J. D. Pack, Special points for Brillouin-zone integrations, Phys. Rev. B **13**, 5188 (1976).

[31] S. J. Blundell, Muon-spin rotation studies of electronic properties of molecular conductors and superconductors, Chemical reviews **104**, 5717 (2004).

[32] J. H. Brewer, S. R. Kreitzman, D. R. Noakes, E. Ansaldo, D. R. Harshman, and R. Keitel, Observation of muon-fluorine" hydrogen bonding" in ionic crystals, Physical Review B **33**, 7813 (1986).

[33] J. S. Lord, S. P. Cottrell, and W. G. Williams, Muon spin rotation in strongly coupled systems, Physica B **289–290**, 495 (2000).

[34] R. Kadono, K. Shimomura, K. H. Satoh, S. Takeshita, A. Koda, K. Nishiyama, E. Akiba, R. M. Ayabe, M. Kuba, and C. M. Jensen, Hydrogen bonding in sodium alanate: a muon spin rotation study, Physical review letters **100**, 026401 (2008).

[35] T. U. Ito, A. Koda, K. Shimomura, W. Higemoto, T. Matsuzaki, Y. Kobayashi, and H. Kageyama, Excited configurations of hydrogen in the $BaTiO_{3-x}H_x$ perovskite lattice associated with hydrogen exchange and transport, Physical Review B **95**, 020301 (2017).

[36] J. M. Wilkinson and S. J. Blundell, Information and decoherence in a muon-fluorine coupled system, Phys. Rev. Lett. **125**, 087201 (2020).

[37] B. N. Figgis and R. L. Martin, 746. Magnetic studies with copper(ii) salts. part i. anomalous paramagnetism and δ-bonding in anhydrous and hydrated copper(ii) acetates, J. Chem. Soc. , 3837 (1956).

[38] V. Vedral, M. B. Plenio, M. A. Rippin, and P. L. Knight, Quantifying entanglement, Physical Review Letters **78**, 2275 (1997).

[39] B. Huddart, A. Hernández-Melián, T. Hicken, M. Gomilšek, Z. Hawkhead, S. Clark, F. Pratt, and T. Lancaster, MuFinder: A program to determine and analyse muon stopping sites, Comput. Phys. Commun. **280**, 108488 (2022).

[40] E. Roduner and H. Fischer, The evolution of muon spin polarization in muonic radicals and related species, Chem. Phys. Lett. **65**, 582 (1979).

[41] J. S. Lord, I. McKenzie, P. J. Baker, S. J. Blundell, S. P. Cottrell, S. R. Giblin, J. Good, A. D. Hillier, B. H. Holsman, P. J. C. King, T. Lancaster, R. Mitchell, J. B. Nightingale, M. Owczarkowski, S. Poli, F. L. Pratt, N. J. Rhodes, R. Scheuermann, and Z. Salman, Design and commissioning of a high magnetic field muon spin relaxation spectrometer at the isis pulsed neutron and muon source, Review of Scientific Instruments **82**, 073904 (2011).

[42] P. Hauke, M. Heyl, L. Tagliacozzo, and P. Zoller, Measuring multipartite entanglement through dynamic susceptibilities, Nature Physics **12**, 778 (2016).

[43] P. Laurell, A. Scheie, E. Dagotto, and D. A. Tennant, Witnessing entanglement and quantum correlations in condensed matter: A review, Advanced Quantum Technologies **8**, 2400196 (2024).